Chapter 5

Data Analysis, Results, and Discussions

From the previous chapter, our results from the CMS simulation chain are stored in DST format. We extracted the particles' information using DST reading feature implemented in ORCA. The operation is described in "Analysis with DST" section below.

5.1 Analysis with DST

The version of ORCA we used in our work is 8.4.0. To perform data analysis on DST, we follow three steps:

1. Specify configuration: RecQuery/RecConfig
2. Obtain reconstructed objects: RecCollection
3. Select interesting reconstructed objects: FilteredRecCollection

The C++ code written to extract information of muons from DST database is shown in Appendix C.

In our work, we are interested in muons from two stages of the simulation chain: the simulated (sim) muons and reconstructed (rec) muons. The simulated muons are output muons from OSCAR. They include any muons that could possibly be produced by any interactions inside the detector. These simulated

muons are not yet being digitized, i.e. no electronic response effect is included. The reconstructed muons are the final output muons from ORCA. These muons are fully reconstructed, digitized and simulated. They are specifically selected by the Trigger algorithm in "Global Muon Trigger" level (GMT), under the trigger selection requirement. The GMT combines the results from two trigger subsystems implemented in the Drift Tube (DT), Resistive Plate Chambers (RPC), and Cathode Strip Chambers (CSC) of the CMS Muon Chamber, and delivers the best muon candidates for users to do data analysis. A diagram showing the CMS muon trigger system is illustrated in Fig. 5.1.

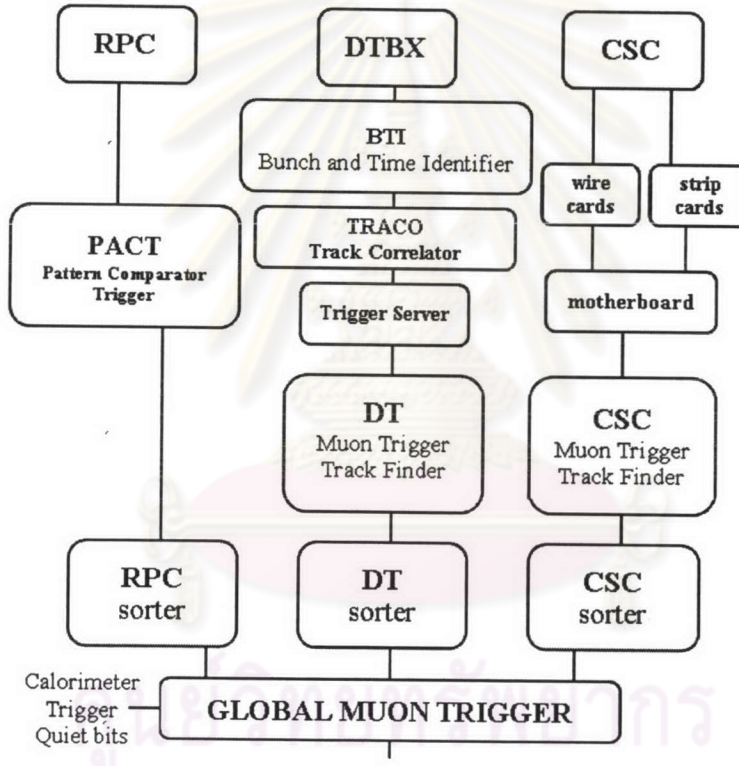

Figure 5.1: The CMS muon trigger system. (picture from the CMS Collaboration, *The Trigger and Data Acquisition Project*, CERN/LHCC 2000-038.)

The class interface and documentation about class method can be found in ORCA Reference Manual [32].

After DST analysis, we finally obtained ntuple files in *ROOT* format which will be analyzed by ROOT, an object-oriented analysis framework [33].

5.2 Analysis with ROOT

Root file is a kind of ntuple file that is used by ROOT program to do data analysis. Data obtained from particle physics experiment are commonly stored in ntuple file format. An ntuple file is a high level data storage for which one of its entry contains "n" pieces of data. For example, in an ntuple file of track information, each of its entry may contain information on charge, momentum, azimuthal angle, polar angle, mass of particles, and number of hits. With some manipulation on the ntuples – for example: selection cuts, several types of plots, curve fitting – interesting physics is revealed through output histograms.

In the past, ntuple file analysis is mostly done by PAW (Physics Analysis Workstation), a FORTRAN based program. Today, with the creation of object-oriented technology, several new tools are invented for handling ntuple and start to replace PAW. One of the most popular is ROOT [33]. Unlike PAW, ROOT is based on C++ object oriented technology. Its advantage over PAW is its capability to handle an impressive amount of data flow expected from LHC and it is a "faster and more efficient [33]" tool for ntuple manipulation.

The results obtained from ROOT are displayed and discussed in the following sections.

5.3 Results and Discussions

In the most recent investigations on studying the possibility of using $W^{\pm}$ and Z^0 as luminosity monitor [15], [16], the results do not include the effect from detector smearing, electronics response and background studies. In our work, we have performed a full chain of CMS simulation on $W^{\pm}$ and Z^0 production and its background candidates. The final output from the simulation were in ROOT file format. We then plotted histograms from the ROOT files for three physical

quantities: P_T, η and ϕ for the muons and tried to analyze these plots. The discussion of the results are divided into seven different topics: 1) Characteristics of Muons from $W^{\pm}$ and Z^0, 2) Comparison between Signal muons and Background muons, 3) The Invariant Mass Plots of Di-muons, 4) Detection Efficiency and Acceptance and 5) Reconstruction Efficiency and Acceptance.

5.3.1 Characteristics of muons from Z^0 and $W^{\pm}$

Understanding the characteristics of muons from $W^{\pm}$ and Z^0 will help us apply good selection criteria to choose the best muons for calculating the luminosity.

From 1,000 of $q\bar{q} \rightarrow Z^0 Z^0 \rightarrow 2\mu^+ 2\mu^-$ events input into OSCAR and ORCA, we made plots for distribution of P_T, η and ϕ of generated, simulated and reconstructed muons. P_T is a transverse momentum defined as

$$P_T = \sqrt{P_x^2 + P_y^2}. \tag{5.1}$$

η is the pseudorapidity, or shortly called "rapidity"; and ϕ is the azimuthal angle. Some explanations and illustrations of the transverse momentum (P_T), pseudorapidity (eta), and azimuthal angle (ϕ) can be found in Appendix A.

The results of the plots for Z^0 are shown in Fig. 5.2, Fig. 5.3 and Fig. 5.4; same kind of plots for muons from $q\bar{q} \rightarrow W^+W^- \rightarrow \mu^{\pm}\nu_{\mu}(\bar{\nu}_{\mu})$ are also shown in these figures.

From the histograms, we found that these muons from $W^{\pm}$ and Z^0 have their P_T distributions in similar shape. Both of their P_T distribution mostly lie in the range of $0 < P_T < 150$ GeV/c, with highest number of aggregation at about 40 GeV/c. This result is in good agreement with the characteristics of muons coming from $W^{\pm}$ and Z^0 bosons in hadron collision at TeV scale [34]. The result also shows that the CMS can successfully trigger and reconstruct muons of high transverse momentum.

In the rapidity distribution, muons from Z^0 tend to form a peak around 0 GeV/c; while for those of $W^{\pm}$, they do not show a clear peak. The peak implies that muons from Z^0 are more perpendicular to the beam line, or, in other words,

central in rapidity. This is also in good agreement with the transversal nature of muons from Z^0 produced at hadron collision at TeV scale [34]. For the case of $W^{\pm}$, we need to run more events to see whether there is a peak similar to the case of Z^0.

In the azimuthal angle distribution, we found that muons from $W^{\pm}$ and Z^0 are distributed at all values of ϕ, from 0° to 360°, with is no preference in any directions.

In summary, for this analysis section, we found that muons from $W^{\pm}$ and Z^0 are high transverse momentum muons and distributed over all angles of the plane perpendicular to the beam direction. Muons from Z^0 are also central in rapidity. Howeverr, for muons from $W^{\pm}$, we still need more number of simulated events to make justification.

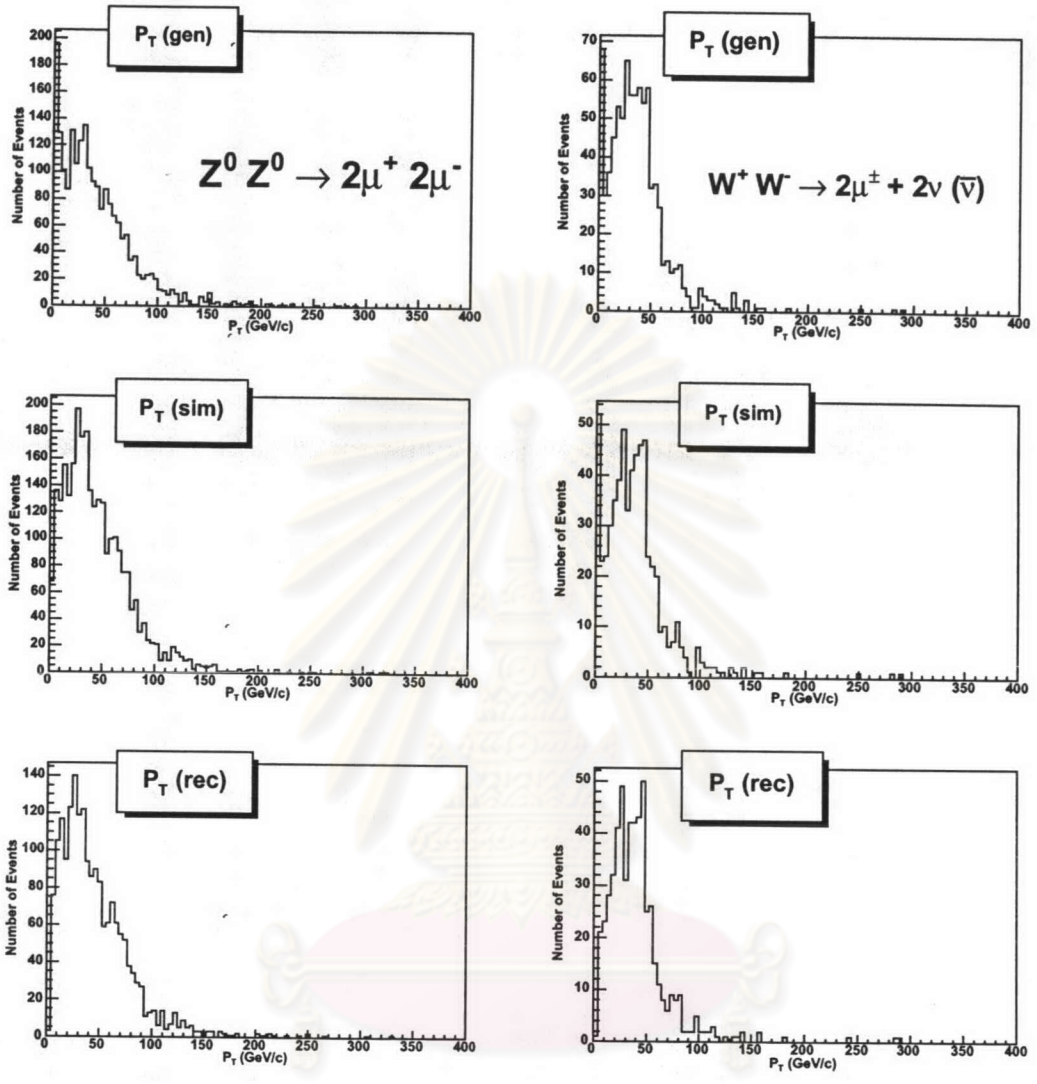

Figure 5.2: The P_T distribution of muons from generated Z^0 (left) and generated $W^{\pm}$ (right).

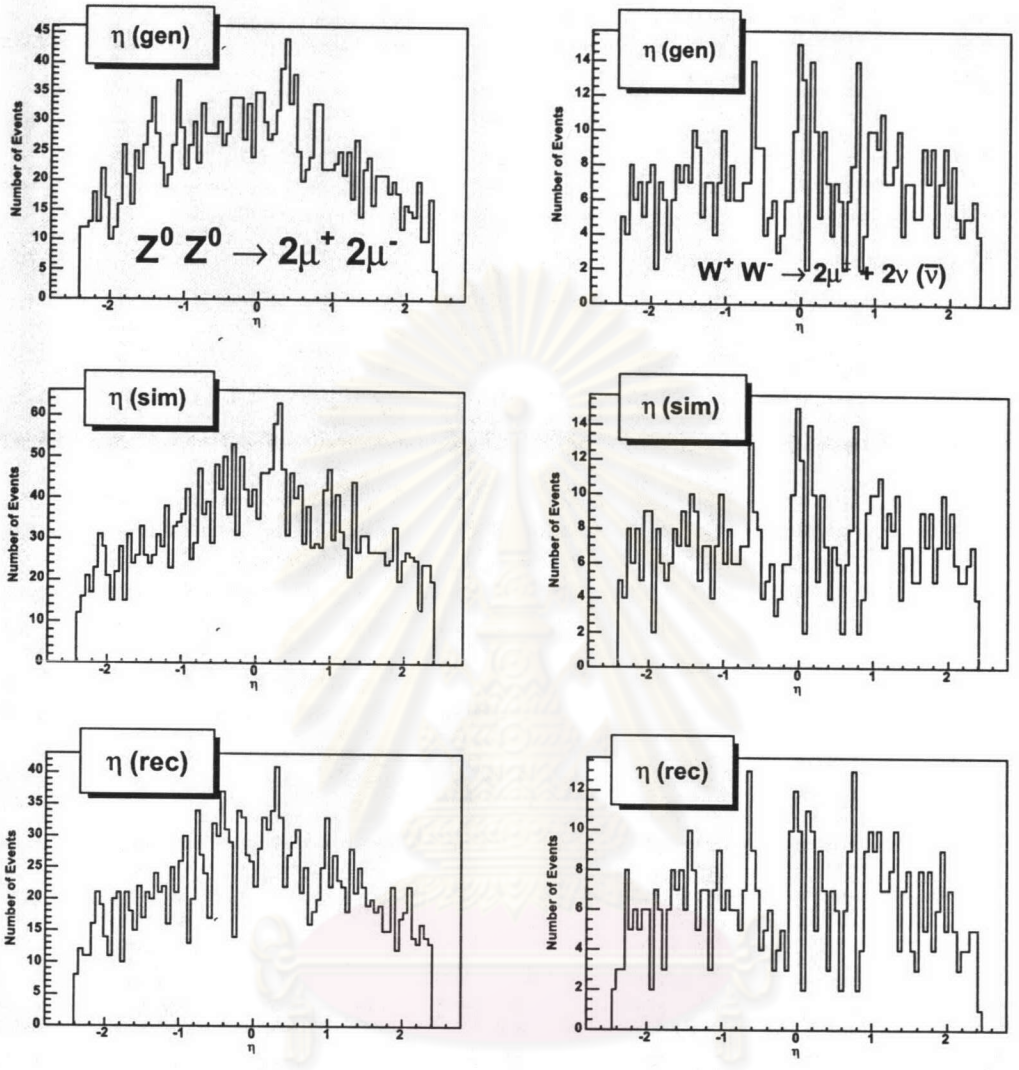

Figure 5.3: The η distribution of muons from generated Z^0 (left) and generated $W^{\pm}$ (right).

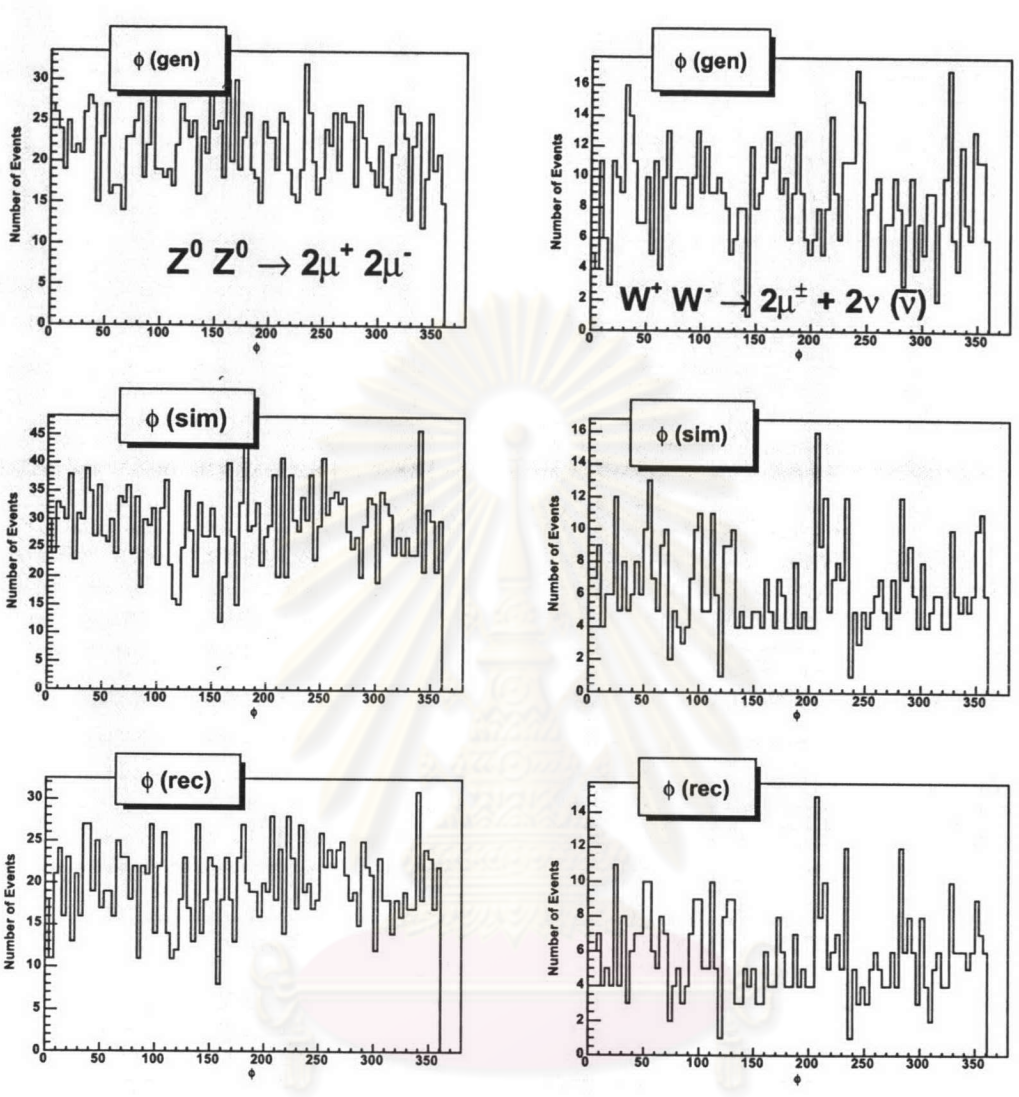

Figure 5.4: The ϕ distribution of muons from generated Z^0 (left) and generated $W^{\pm}$ (right).

5.3.2 Comparison between Signal Muons and Background Muons

In this section, we present comparisons between muons from signal ($W^{\pm}$ and Z^0 production) and muons from background processes (Drell-Yan, $\gamma^*\gamma^* \rightarrow \mu^-\mu^+$, $\gamma\gamma \rightarrow \mu^-\mu^+$ and minimum bias processes). The histograms are displayed in Fig. 5.5, Fig. 5.6 and Fig. 5.7. The distinction in their distributions will be useful in data analysis work involving the signal-background isolation. In particular, to be able to efficiently distinguish between muons from the weak boson production and muons from the background processes will ensure us that the muons that we count to obtain the event rate ($R_{evt} \equiv$ number of muons produced per second) for calculating the luminosity (using equation $\mathcal{L} = R_{evt}/\sigma$) are certainly muons from the $W^{\pm}$ and Z^0 particles. In addition, this comparison analysis will be useful in the Higgs search for decay channels $H \rightarrow Z^0Z^0 \rightarrow 4l^{\pm}$ and $H \rightarrow W^+W^- \rightarrow l^{\pm}\nu(\bar{\nu})$.

The discussions of this section is only presented for generated muons. For for the cases of simulated and reconstructed muons, we postpone them for future work due to large amount of time required to run all the background processes through simulation and reconstruction.

For the generated muons, the most obvious distinction between signal and background lies in the transverse momentum distribution. From Fig. 5.5, we see that P_T distributions of muons from $W^{\pm}$ and Z^0 are high ($0 < P_T < 120$ GeV/c) compare to P_T distributions from other backgrounds ($0 < P_T < 6$ GeV/c), except for the Drell-Yan background. The clear distinction in P_T values show that if we impose constraint on $P_T > 6$ GeV/c of the muons, we will be able to efficiently remove all low transverse momentum background from the $W^{\pm}$ and Z^0 signal.

However, for the Drell-Yan background, even though its P_T distribution is not as high as those of Z^0 and $W^{\pm}$, there is some possibility that it can significantly contaminate the signal of $W^{\pm}$ and Z^0 due to its P_T distribution range, $0 < P_T <$ 20 GeV/c. We need to investigate how much does it contaminate $W^{\pm}$ and Z^0. The investigation to find the Drell-Yan contamination is shown in the next analysis section.

In Fig. 5.6, the rapidity distribution comparison of the generated muons is

displayed. The figures show that the background have their η distributions with no obvious peak. On the other hand, the rapidity distributions of muons from Z^0 tends to form a peak at $\eta = 0$. Muons from $W^{\pm}$ do not form a clear peak, supposedly because there are too few of them. This finding shows that we cannot use η cut as a tool for removing the Drell-Yan background.

In Fig. 5.7, the azimuthal angle distributions of generated muons from both signal and background do not show obvious distinction.

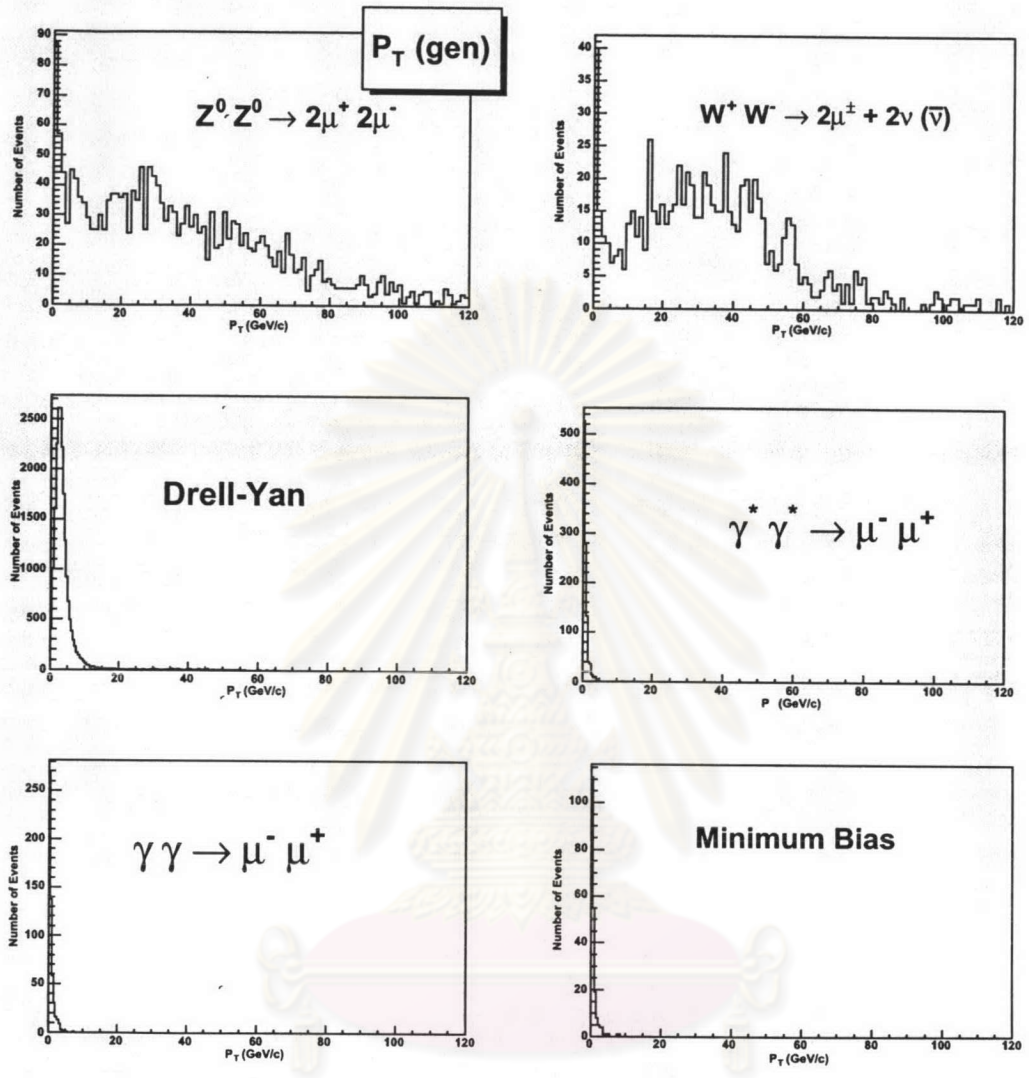

Figure 5.5: Comparison of P_T distribution between generated signal and background

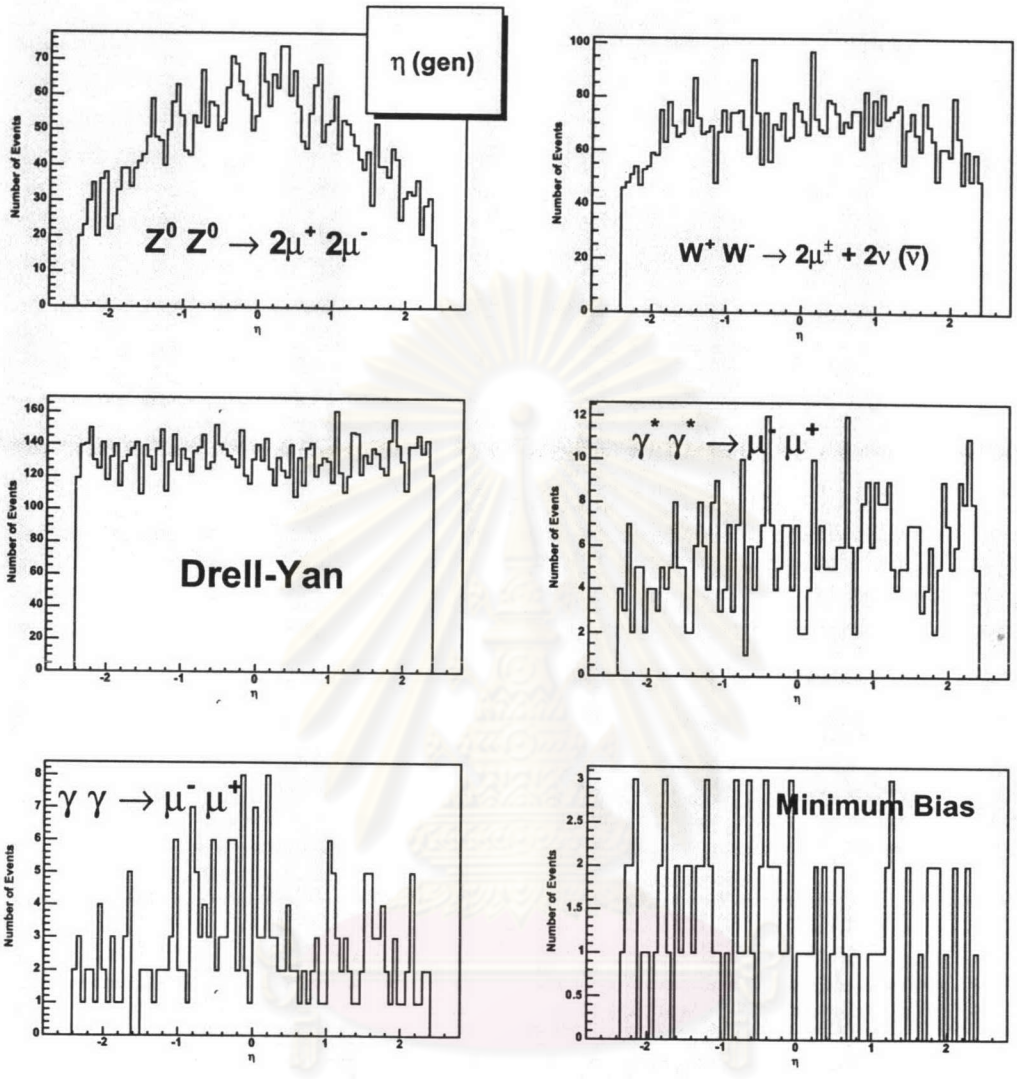

Figure 5.6: Comparison of η distribution between generated signal and background

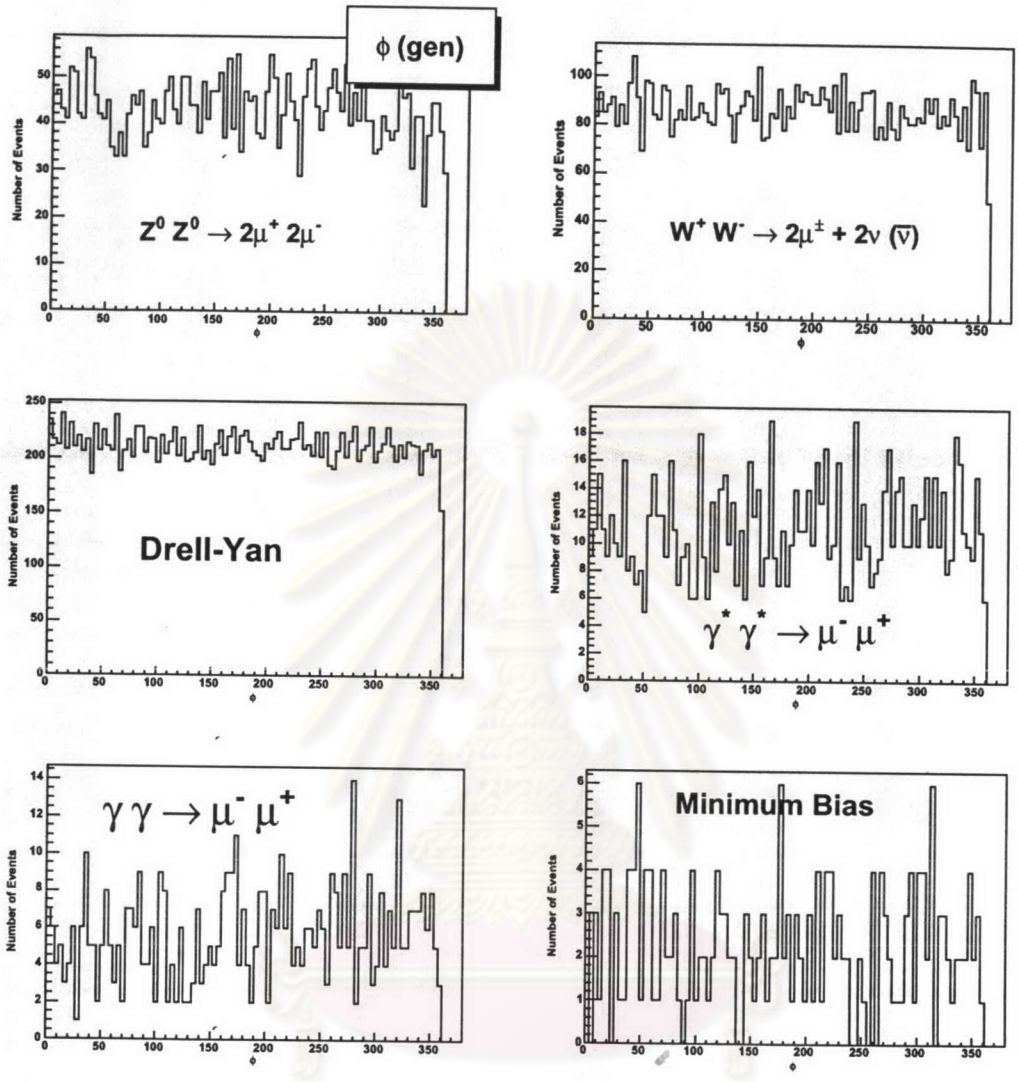

Figure 5.7: Comparison of ϕ distribution between generated signal and background

5.3.3 The Invariant Mass Plots of Di-muons

The Invariant Mass Plots of Z^0

We have also made an invariant mass plots for the generated and reconstructed Z^0, as shown in Fig. 5.8. The Gaussian fit was applied over the range $75 < M_{\mu^+\mu^-} < 105$ GeV/c^2, which is standard for the Z^0 mass window. We obtain the following meas values:

$$M^{gen}_{\mu^+\mu^-} = 91.34 \pm 0.05 \text{ GeV/c}^2$$
$$M^{rec}_{\mu^+\mu^-} = 91.34 \pm 0.14 \text{ GeV/c}^2.$$

The values are slightly different ($\sim 0.32\%$ errors for both generated and reconstructed Z^0) from the most recent accepted value [2], where $M_{Z^0} = 91.1876 \pm 0.0021$ GeV/c^2. The results for generated and reconstructed invariant mass are very close. This results verify that we have had a good reconstruction process in our work.

The Drell-Yan Background Analysis

As stated earlier in the last analysis section, we want to know how much the Drell-Yan background contaminate our count of Z^0 and $W^{\pm}$. In order to find the contamination, we used PYTHIA 6.2 to generate the process $q\bar{q} \rightarrow \gamma^*/Z^0 \rightarrow \mu^+\mu^-$ and plotted the invariant mass of di-muons from Z^0 and the Drell-Yan process. The invariant mass, $M_{\mu^+\mu^-}$, of the di-muons can be found from a formula

$$M_{\mu^+\mu^-} = \sqrt{(E_{\mu^+} + E_{\mu^-})^2 - (P_x^{\mu^+} + P_x^{\mu^-})^2 - (P_y^{\mu^+} + P_y^{\mu^-})^2 - (P_z^{\mu^+} + P_z^{\mu^-})^2}. \quad (5.2)$$

For $W^{\pm}$, we have not yet been able to construct its invariant mass because of neutrino related problem. Consequently, we omitted the $W^{\pm}$ invariant mass plot for future work.

The results of the invariant mass plots for generated Z^0 and Drell-Yan are shown in Fig. 5.9. In this figure, the Drell-Yan invariant mass mostly aggregates at low-mass value, $5 < M_{\mu^+\mu^-} < 30$ GeV/c^2 (5 GeV/c^2 is the cutoff value of the Drell-Yan

in the event generation process to avoid wasting large amount of time to generate muons at 0 GeV/c^2). On the other hand, the Z^0 invariant mass aggregate at about 91 GeV/c^2 with much smaller peak compare to the Drell-Yan. The two aggregations are clearly separated, which convince us that an invariant mass cut can be an efficient tool to isolate low-mass Drell-Yan background from the Z^0 signal. Imposing a cut on standard Z^0 mass window ($75 < M_{\mu^+\mu^-} < 105$ GeV/c^2) yield an integral number of 2146 events from the total of 998390 generated events.

However, if we look closer to the Drell-Yan tail in the range of Z^0 mass window, as shown a lower picture of Fig. 5.9, the tail of the low-mass Drell-Yan can contaminate Z^0 signal. This contamination could result in inaccurate count of the number of Z^0, which will consequently effect the precision of luminosity measurement. To find how much does the Drell-Yan tail effect the count of Z^0, we tried fitting a curve of the low-mass Drell-Yan, using polynomial degree 9 fit in ROOT program. Under the polynomial fit curve, we found that there are approximately 298 events of Drell-Yan background in the Z^0 mass window ($75 < M_{\mu^+\mu^-} < 105$ GeV/c^2). An illustrations shown our fittings are depicted in Fig. 5.10.

298 events is $\approx 298 \div 2146 \approx 13.89\%$ of the whole Z^0 events in the Z^0 mass window. When we calculate the luminosity by using the Z^0 production, this number should be taken into account.

After we subtracted the Drell-Yan's tail in the Z^0 mass window, we plotted the subtracted signal as shown in Fig. 5.11. The Gaussian fit was applied to the histogram and yielded a mean value:

$M^{Z^0}_{\mu^+\mu^-} = 90.76 \pm 0.04$ GeV/c^2.

This result is $\sim 0.47\%$ error from the recent accepted value [2].

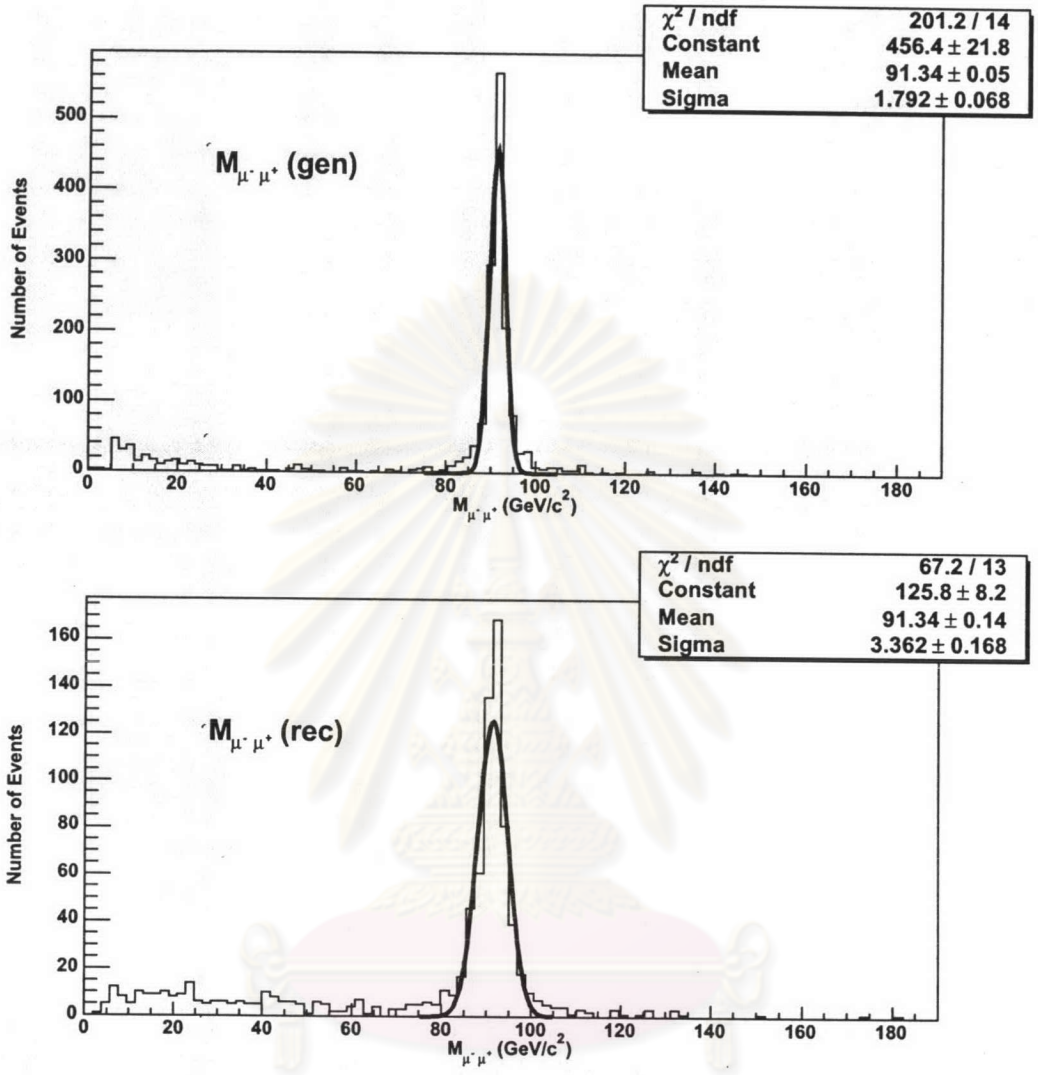

Figure 5.8: The invariant mass plot of di-muons from simulated and reconstructed Z^0.

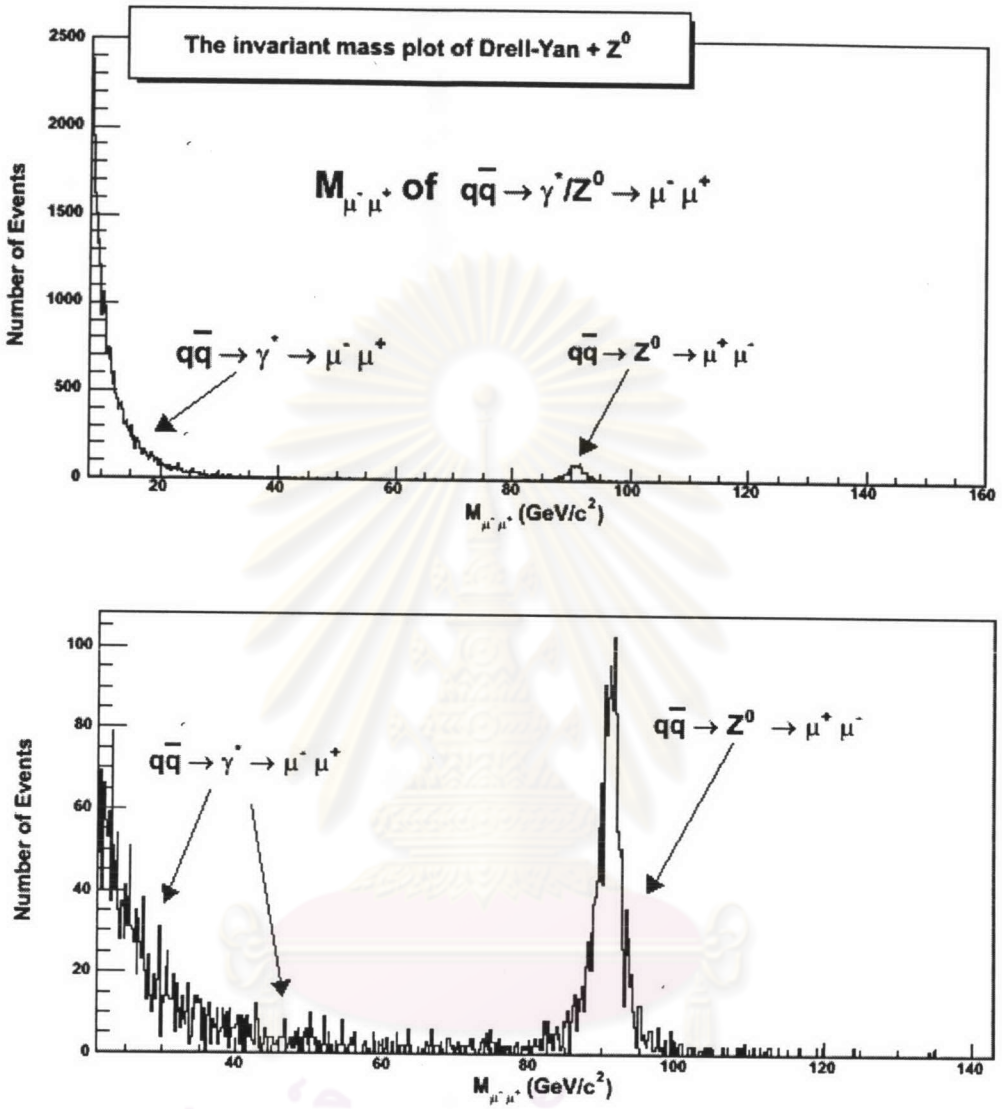

Figure 5.9: The invariant mass plot of di-muons from generated low-mass Drell-Yan and generated Z^0.

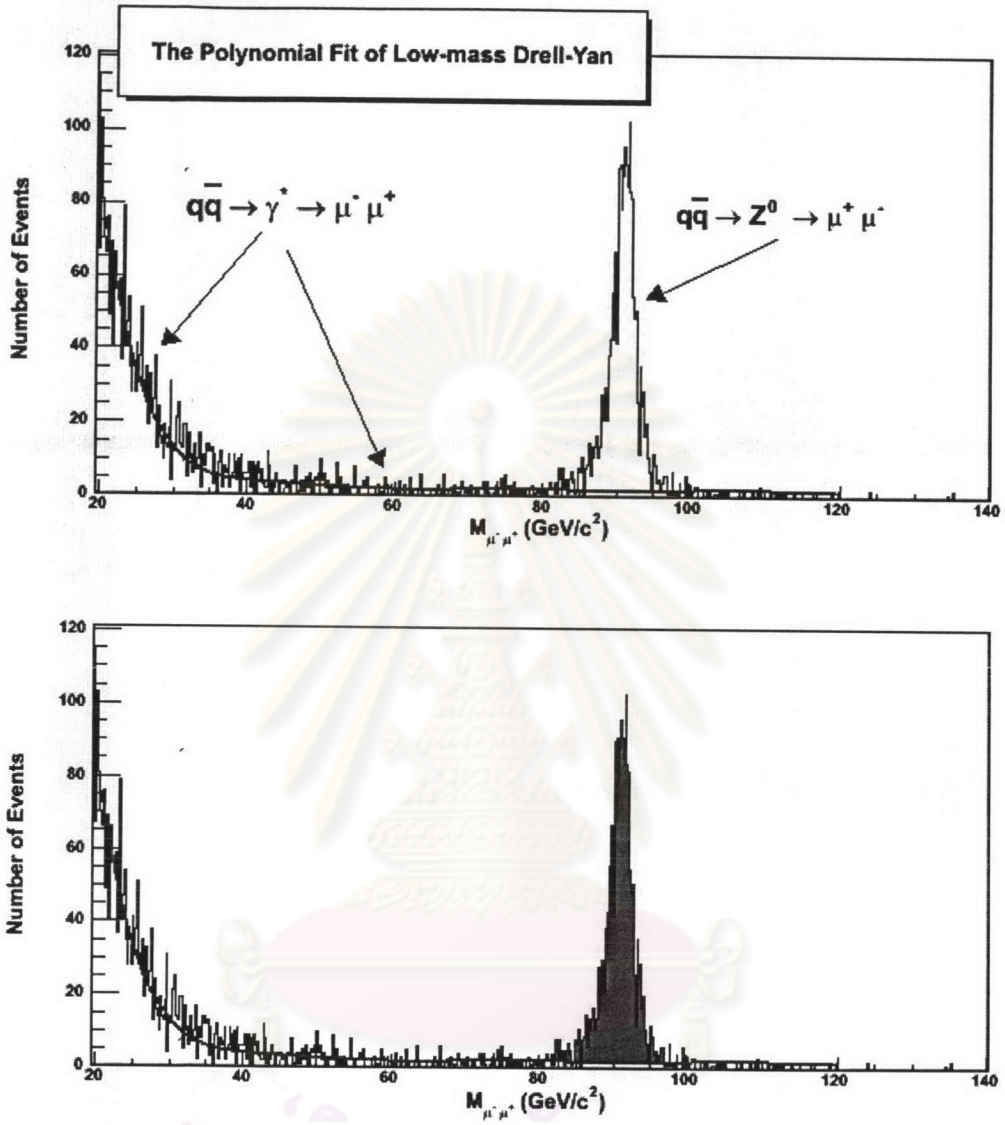

Figure 5.10: The polynomial fit on generated low-mass Drell-Yan.

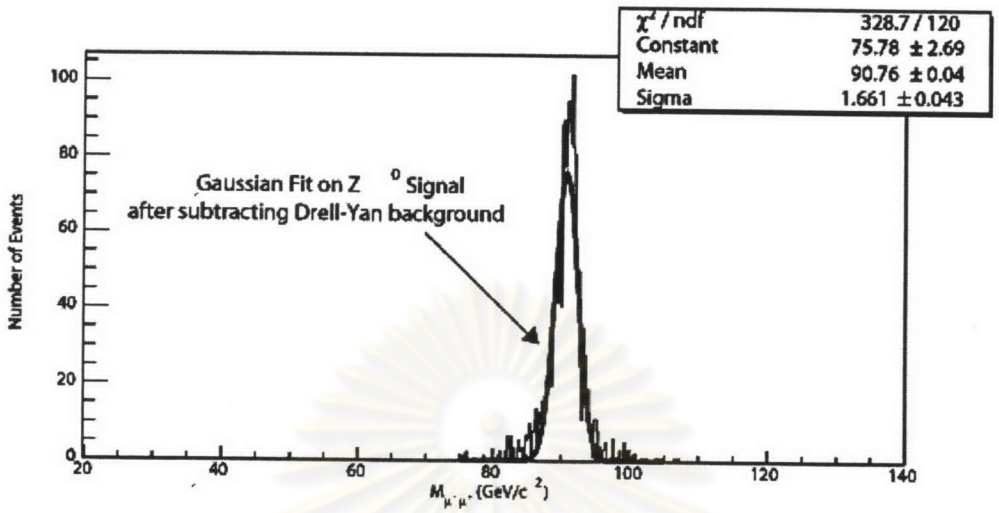

Figure 5.11: The Z^0 signal after subtracting the Drell-Yan's tail.

5.3.4 Reconstruction Efficiency and Acceptance

The luminosity will be effected by the reconstruction efficiency from a relation:

$$\mathcal{L} = \frac{R_{evt}}{\sigma \cdot \mathrm{Eff}_{tot}} \tag{5.3}$$

where Eff_{tot} is the total efficiency ($\mathrm{Eff}_{tot} = \mathrm{Eff}_{rec} \cdot \mathrm{Eff}_{sel} \cdot$ .....).

For the reconstruction efficiency, we have

$$\mathrm{Eff}_{rec} = \frac{N_\mu^{rec}}{N_\mu^{gen}} \tag{5.4}$$

where N_μ^{gen} is the number of generated muons and N_μ^{rec} is the number of reconstructed muons. The results from our calculation for Z^0 and $W^\pm$ reconstruction efficiency are displayed in Table 5.1.

Table 5.1 show that the reconstruction process has $\sim$ 90% efficiency for muons from Z^0. This is in agreement with the $>$ 90 % efficiency of the muon reconstruction design of the CMS detector [35]. For the case of $W^\pm$, further investigations are needed to check whether there are errors in our reconstruction

Table 5.1: The reconstruction efficiency of muons from Z^0 and $W^{\pm}$.

Process	number of gen muons	number of rec muons	efficiency
$q\bar{q} \rightarrow Z^0 Z^0 \rightarrow 2\mu^+ 2\mu^-$	2065	1885	91.28%
$q\bar{q} \rightarrow W^+ W^- \rightarrow \mu^{\pm}\nu_{\mu}(\bar{\nu}_{\mu})$	826	552	66.83%

algorithm or programming problems in the stage of reconstruction. However, to determine that how large does the reconstruction effect the luminosity estimation using $W^{\pm}$ and Z^0 production, we still need much more number of events input into OSCAR and ORCA, to obtain much better statistical results.

In geometric acceptance of the reconstruction system, we have the same conclusion as the case of simulation. As shown in Fig. 5.3 and Fig. 5.4, we have obtained good acceptance for all values of rapidity range $|\eta| < 2.4$, and azimuthal angle.